2013 IEEE/RSJ International Conference on
Intelligent Robots and Systems (IROS)
November 3-7, 2013. Tokyo, Japan

A Jumping Robotic Insect Based on a Torque Reversal Catapult Mechanism

Je-sung Koh, *Student Member, IEEE* Sun-pil Jung,
Robert J. Wood, *Member, IEEE* and Kyu-jin Cho, *Member, IEEE*

***Abstract*— The design and the fabrication of a mesoscale jumping robotic insect are presented. The basis of the robot is a torque reversal catapult mechanism, inspired by a flea's jumping leg. The current robot structure is 20mm in length, 2mm in height and weighs 34mg. The smart composite microstructures (SCM) process is used to developing the mesoscale structures and articulated, flexure-based mechanisms of the leg. Furthermore, the design is compatible with the pop-up book MEMS process, ameliorating the laborious assembly process of small components. The robot prototype can achieve jumps of approximately 30cm with a 2.7m/s initial velocity. It is 150 times its body height. The effect of air resistance is considered in order to improve jumping performance with the light weight body structure. The air resistance efficiency (Jumping height in air (h_v) / Jumping height in vacuum (h_v)) is computed to be 0.83 and the robot exhibits a drag coefficient of 1.8.**

I. Introduction

Previously, two types of jumping mechanisms have been developed based on the torque reversal principal inspired by fleas. The first one was 2cm long, weighing 1.104 grams and jumped 64cm [1]. The second prototype had a simplified 10mm low profile jumping shape and could jump 1.2m [2]. Fig 1. (a) and (b) show schematic designs of these two previous mechanisms. The unique jumping mechanism of the flea's leg inspired the development of these meso-scale robotic jumping insects. The basis of these robots is a torque reversal mechanism – a catapult mechanism – that rapidly transfers stored elastic energy into kinetic energy. With a muscle or a smart actuator that can change its stiffness, it is categorized as an active storage and active release catapult mechanism in Table I [2]. The torque reversal mechanism is composed of three main components; an extensor muscle, a stopper, and a triggering muscle.

This research was supported by the Research Center Programs through the National Research Foundation of Korea (NRF) funded by the Ministry of Education, Science and Technology (2012K001368, 2009-0087640).

J. S. Koh and S. P. Jung are with the Biorobotics Laboratory, School of Mechanical & Aerospace Engineering, Seoul National University, Seoul, Republic of Korea (email : kjs15@snu.ac.kr, sunpill20@snu.ac.kr)

R. J. Wood is with the School of Engineering and Applied Sciences and the Wyss Institute for Biologically Inspired Engineering, Harvard University, Cambridge, MA 02138 (rjwood@eecs.harvard.edu)

K. J. Cho is with the Biorobotics Laboratory, School of Mechanical & Aerospace Engineering/IAMD, Seoul National University, Seoul, Republic of Korea (corresponding author to provide phone: 82-2-880-1663; e-mail: kjcho@snu.ac.kr).

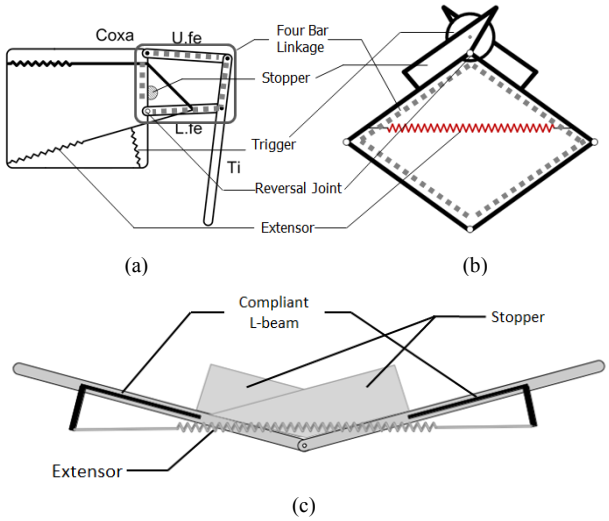

Figure 1. Schematic designs of the torque reversal catapult mechanisms. (a) first prototype of active storage and active release mechanisms [1], (b) second prototype [2], (c) current active storage and passive release mechanism.

Compared to other catapult mechanisms, which commonly have latches (e.g. small pin-like elements or friction detents) the torque reversal mechanism presented in this paper utilizes a bistable structure to store and rapidly release elastic energy. This is an advantage for miniaturization since such a mechanism doesn't need small mechanical elements for a latch or precision friction, both of which are hard to repeatable produce on the millimeter scale. The previous two robot mechanisms demonstrated the feasibility of developing a small scale jumping robot with the torque reversal mechanism inspired by the flea's jumping leg.

The Smart Composite Microstrucures (SCM) process is applied to produce the millimeter- scale flexure-based linkages of the jumping mechanism. This process creates laminated composites of bulk-machined materials that form

TABLE I. Categorization of Catapult Mechanisms

Symbol	Passive Storage	Active Storage
Passive Release	Grillo [6] 7g robot [7] Closed elastic [8] Jollbot [9] Mini-Whegs [10] L. Xiao *et al.* [11]	**Design in this paper**
Active Release	Circular robot [12] Jumping microrobot [13] Hooper [14]	FLEA v1 [1], v2 [2]

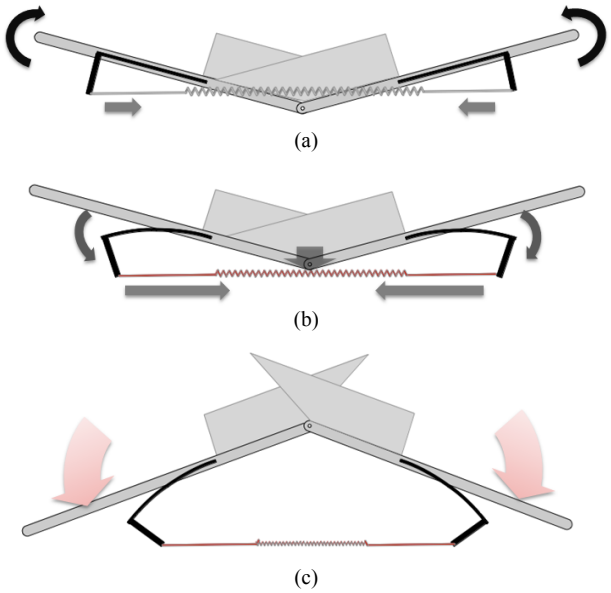

Figure 2. The jumping process for the current design.

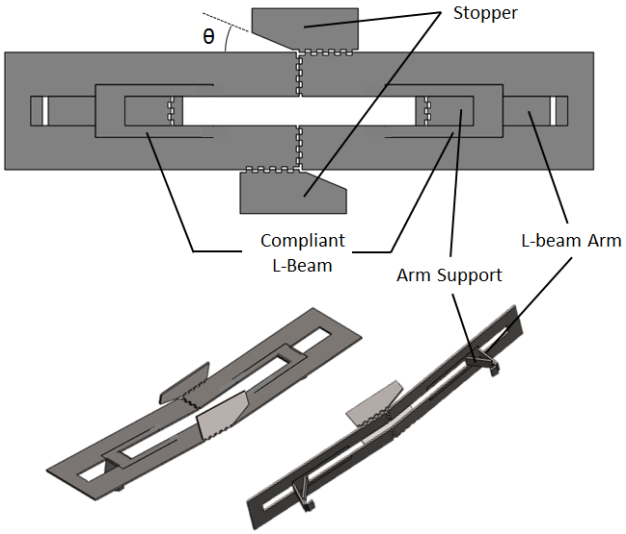

Figure 3. The planar design (top) and folded shape (bottom) of the body structure.

structures and mechanisms based on folded flexure joints with feature sizes ranging from micrometer to centimeter [3]. The quality of the SCM is improved by using cured carbon composites and adhesive layers in the process. It reduces problems caused by misalignment of prepregs during layering and the overflow of the resin during the curing process. Furthermore, folding is automated by using pop-up book MEMS techniques [4].

In this paper, a smaller and lighter torque reversal mechanism design is introduced and the design is compatible for applying the SCM and pop-up book MEMS processes. The current design has simple structure by removing the triggering actuator from the previous design [2]. It is replaced by a passive triggering mechanism which is described in detail in the following section. A thin, laser-cut sheet SMA actuator is employed as the extensor actuator. It is a suitable actuator for millimeter-scale robots and compatible with the SCM and pop-up book MEMS processes considering its high energy density and thin profile.

The experimental results show that the robot jumps approximately 30cm with a 2.7m/s initial velocity. The effect of air resistance is analyzed by measuring the jumping efficiency (0.83). As expected, in small, light jumping robots, air resistance significantly affects jumping height and jumping efficiency [5].

II. Design of The Jumping Robotic Insect

A. Catapult Mechanism Inspired by a Flea's Jumping Leg

Expanding upon previous research [1, 2], a third proposed jumping mechanism is shown in Fig.1 (c). It is simplified to contain only three essential components, each compatible with the SCM and pop-up book MEMS manufacturing and assembly processes. The manufacturing process is described in detail in the following fabrication section.

Comparing the three jumping mechanisms in Fig. 1, it is clear that the mechanisms become simpler and more compact through the removal of redundant elements. In the second prototype (fig.1 (b)) the Coxa structures and the long legs are removed from the first design (Fig. (a)). In the current design, the triggering actuator is replaced by a compliant L-beam component. As the L-beam bends, the actuator passes through the center of the rotation, causing the torque to reverse its direction, and allowing the robot to open its legs for jumping. This L-beam incorporates the storage and the triggering components, reducing the number of actuators in the entire system. The linkage structure and stopper are similar to the second design where the stoppers block the two links from bending upward as shown in Fig.1 (c). The extensor is an artificial muscle actuator that can change stiffness. Shape memory alloys are suitable actuators for the torque reversal mechanism due to their temperature-dependent phase transition. In the categorization of the catapult mechanisms shown in Table I [2], the third type can be classified as an active storage and passive release catapult mechanism. Active storage is that elastic energy is stored by increasing stiffness of the elastic material not by deforming the elastic materials. Passive release means that triggering is done passively. In the current design, elastic energy is stored in the extensor and L-beam by increasing the stiffness of the extensor and released automatically by exceeding the critical bending of the compliant L-beam.

The jumping process for the current design goes through three steps as shown in Fig. 2. In the initial position shown in Fig. 2 (a), the extensor has a low stiffness at a low temperature and it can be stretched easily for the mechanism to be the initial position. Therefore, a small torque is exerted upward with respect to the rotation joint at the center of structure. The stoppers block the links and maintain the initial position but the torque is not strong. When the extensor increases stiffness by heating, and thus the pulling force exerted at the arm of the compliant L-beam, the L-beam starts to bend and the extensor moves down as shown in Fig. 2 (b). At this stage, elastic energy is stored in the extensor and the compliant L-beam. Right after the extensor passes through the rotation joint, the direction of torque exerted on the structures is reversed. The

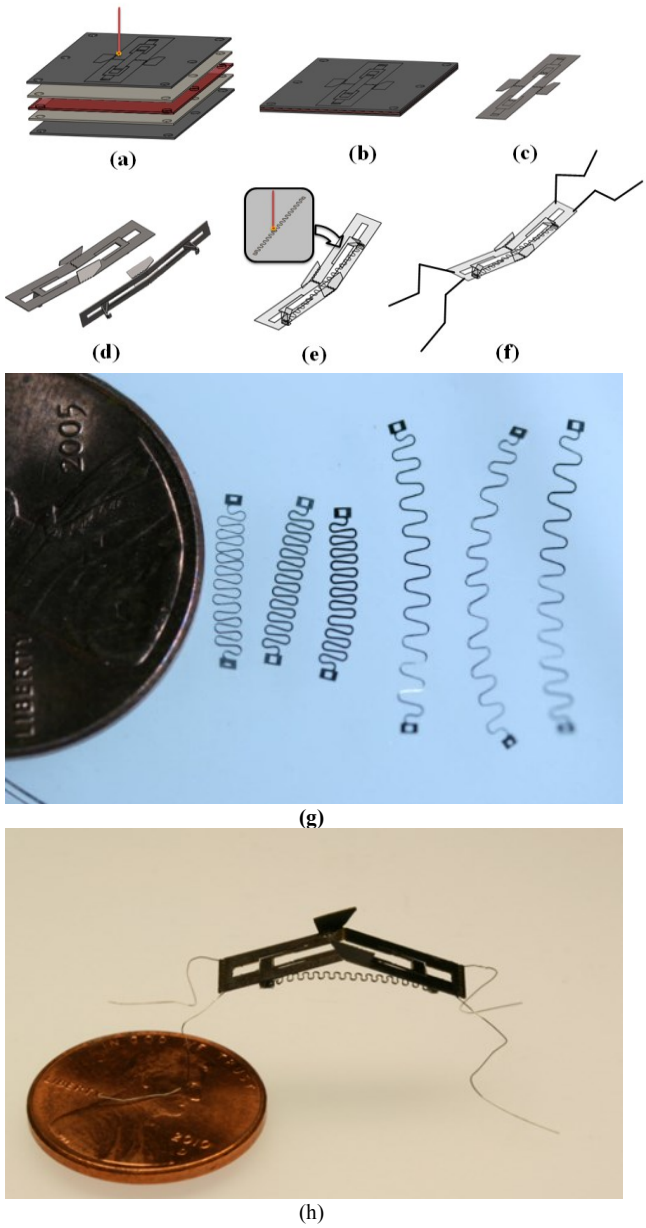

Figure 4. Manufacturing process of the robot structures (a)-(f), the sheet SMA actuators cut by the UV Laser (g), the final prototype (h).

reversed torque rotates the links downward and the stored elastic energy is explodes to rapidly transform into kinetic energy as shown in Fig. 2 (c). As the links rotate, the moment arm – the normal distance between the extensor and the rotation joint – increases and the torque increases rapidly. Finally, the extensor returns to original length and the structure takeoff with the shape of arrow tip. With this mechanism, the two links work as the jumping legs. In order to magnify the rotation radius of the links, we also include longer wire legs in the final prototype.

B. Planar Design for SCM Manufacturing

The robot structure is designed to be compatible with the SCM process described in the following section [3]. This process creates millimeter-scale linkages by laminating multiple sheets of precision laser-machined materials. In this manufacturing process, the planar folding pattern is folded into 3D shape that becomes the final robot. Therefore, a 2D folding pattern design is needed to create the robot structures, unlike traditional mechanical design.

The upper portion in Fig. 3 is the 2D folding pattern design of the current jumping mechanism. The solid line is the cutting line for laser machining. Jagged cutting lines are folding joints connected by a flexible polymer film. This "castellation" shape enables very short length flexures and avoids buckling [4].

The angle θ of the stopper determines the initial shape of the jumping mechanism as shown in Fig. 2 (a). The length of the L-beam arm and the angle θ are the most important design parameters for positioning the extensor. The extensor should be located between the L-beam virtual bending joint and the rotation joint of the links because the L-beam must be bent downward in order to reverse the torque direction. In this prototype, θ is set to 20° and the length of the L-beam arm is 1.7mm in order to position the extensor just above the rotation joint of the links. The arm support is used to distribute the stress at the L-beam folding joint.

The lower portion of Fig. 3 shows the folded structure from the 2D pattern design. The only active joint is the rotation joint at the middle of the structure connecting the two links. The extensor is put at the tip of the L-beam where there are small links for attachment.

III. FABRICATION

As mentioned at the previous section, the robotic jumping insect is fabricated by SCM process which is the laminating process with multiple material layers [3]. Fig. 4 shows the stages of fabrication. Five layers are needed to make the linkage structures; two carbon composite plates, two adhesive layers (FR1500, Dupont Co.), and a single Polyimide film layer (Kapton, Dupont Co.). Each layer is cut by UV laser (355um wavelength) precisely as shown in Fig. 4(a). Each layer has pin alignment holes and is laminated in the following order: carbon composite, adhesive, kapton, adhesive, carbon composite. After aligning, it is pressed and cured at approximately 80psi and 250°C for 3 hours as shown in Fig. (b). The laser is used again to cut the outer line of the layup to release the unassembled robot linkage as shown in Fig. 4 (c). The structure is folded and fixed using Epoxy adhesives as shown in Fig. 4 (d). The actuator is attached to the linkage structure (Fig. 4 (e)).

The extensor is made of a thin sheet of SMA. Due to its thin form factor, sheet SMA is compatible with the lamination process. The SMA has about 8-10% of actuation strain range. In order to amplify the actuation stroke, we cut the sheet SMA into serpentine shapes as shown in Fig. (g) again using the UV laser. With this pattern, the SMA actuator creates greater than 100% actuation strain. Each end of the sheet SMA actuator has small hole to increase adhesion with the robot structure.

The serpentine sheet SMA actuator is attached at the L-beam arm with epoxy adhesives. Finally, we attach four legs for extended ground contact during jumping (Fig. 4 (f)). The

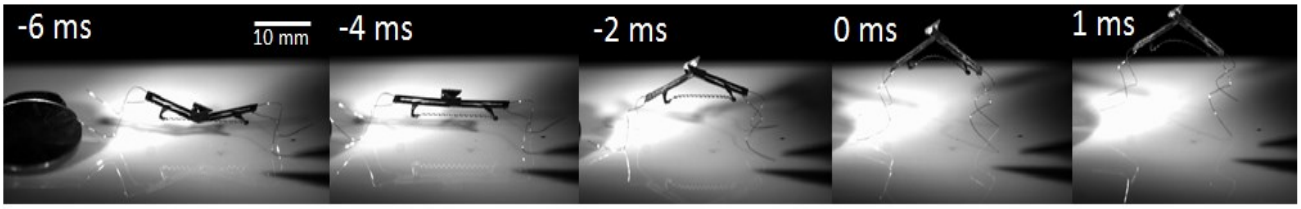

Figure 5. Sequential high-speed video images at takeoff

legs are made of the 3 mil Nickel-Chromium wire. The final prototype is shown in Fig. 4 (h) and detailed specifications of the robot are listed in Table II.

IV. Jumping Performance

A. Heating the Sheet SMA Actuator

The SMA returns to its original shape by phase transformation from Martensite to Austenite phase. Each phase has different mechanical property such as Young's modulus that causes stiffness change. The SMA is activated by heating the actuator above the phase transformation temperature (Austenite start-finish temperature). A common method is Joule heating via an applied electric current. However, this requires a wire tethering which can reduce the jumping height of a small robot. As an alternative, several non-contact heating methods are available such as convection by a hot plate or directed radiation from a laser. In this paper, we use a hot plate to activate the jumping robot. The prototype is just placed on the hot plate and when the temperature of the sheet SMA actuator exceeds the transition temperature, the torque reversal mechanism is triggered automatically. Therefore it can be categorized as an active storage and passive releasing catapult mechanism [1].

B. Jumping Experiment Results

The torque reversal mechanism is triggered a few seconds after being placed on the hot plate. It takes 6 milliseconds to release the elastic energy and take off as shown in Fig. 5. In this figure, we can see that the compliant L-Beam is bent by the extensor actuator. The four wire legs push the robot up – the bent shape of the legs is beneficial for maintaining contact with the ground until takeoff.

The velocity profile during takeoff is measured using high-speed video analysis (ProAnalyst). This profile is plotted in Fig. 6 (a). Since it is difficult to determine the exact center of mass, we measure the velocity of the rotation joint and use this in Fig. 6. The oscillation of the velocity profile is due to leg vibrations immediately after takeoff. The maximum takeoff velocity is approximately 3.5 m/s as shown in Fig. (a). But this is not considered the takeoff velocity of the robot because the velocity of the rotation joint is much higher than that of the center of mass (due to the vibrations). We assume the takeoff velocity is approximately 2.7 m/s, which is extracted from the average oscillation curve.

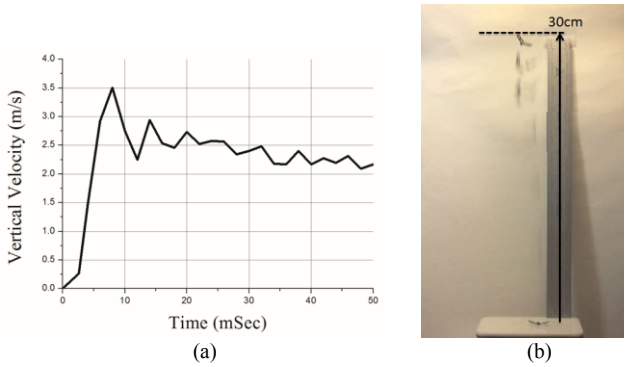

(a)

(b)

Figure 6. (a) Velocity profile at takeoff and (b) jumping profile of the prototype.

After several jumping tests, the maximum jumping height is 30cm as shown in Fig. (b). This is roughly 150 times the robot body height. This value is similar to an actual flea's jumping performance.

This result is based on the initial feasibility test of the micro scale torque reversal catapult mechanism inspired by real flea's jumping mechanism. With this initial result, the design of the robot structure and actuator can be optimized to the effect of air drag.

TABLE II. Spec. of the Micro Robotic Jumping Insect Prototype

Robot weight	34mg	
Overall dimensions	Length	20mm
	Width	2mm
	Hieght (Only structure)	2mm
Composite structure	185 μm (Carbon Composite : 80μm, Kapton : 25μm Adhesive layer : negligible)	
Sheet SMA	Thickness	150μm
	Width	100um
	Initial Length	12mm
	Extended Length	18mm

V. The Effect of Air Resistance

Air drag is primary limiting factor of the jumping height. As the size of light-weight projectiles is decreased, air drag effects play a more dominant role. In H. Bennet-Clark et al. [5], lightweight, small insects have much lower efficiency than the bigger insects when they are thrown with faster velocity. The efficiency is defined as the actual jumping height (h_a) in the air divided by the jumping height in vacuum

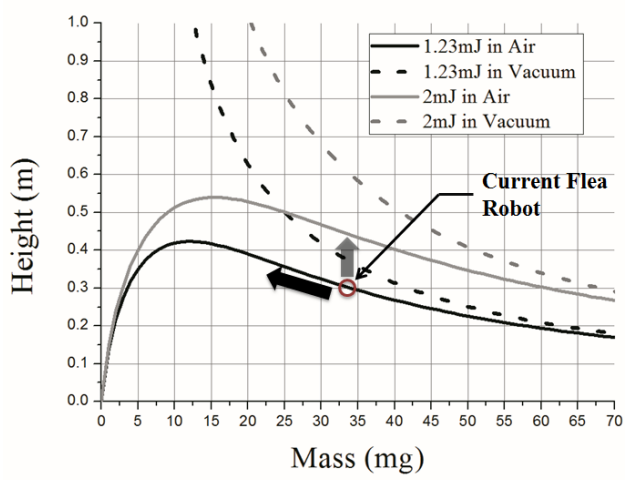

Figure7. Graph of jumping height in air and vacuum versus body mass for different initial kinetic energies.

(h_v). With following equations, we can simulate the effect of the air resistance. The drag force is expressed as follows:

$$F = C_D \rho A v^2 / 2 \tag{1}$$

Where C_D is the drag coefficient, ρ is the density of air, A is frontal cross section area, and v is the body velocity. The dynamic equation of the jumping projectile is written as follows:

$$m \frac{d^2 x}{dt^2} + \frac{C_D \rho A}{2} \left(\frac{dx^2}{dt} \right) + m g_n = 0 \tag{2}$$

Where m is the mass of the body, x is the distance above the ground, t is the time since leaving the ground, and g_n is gravitational acceleration. The solution of equation (2) gives the maximum jumping height in air:

$$h_a = \frac{m}{C_D \rho A} \ln \left[\frac{C_D \rho A v_p^2}{2 m g_n} + 1 \right] \tag{3}$$

The actual jumping height, h_a, and the initial jumping velocity, v_p, can be obtained from experimental results. From the previous section, h_a is 30cm and v_p is 2.7m/s. From equation (3) and with experimental results, C_D, which is a strong function of body shape, is determined to be 1.89. The air drag characteristics of the current design are listed in Table III. In Fig. 7, the maximum height as a function of body mass is plotted in both air and vacuum based on the following relationship:

$$h_v = \frac{v_p^2}{2 g_n} = \frac{E}{m g_n} \tag{4}$$

The position of the current jumping robot is marked with red circle at the mass value of 34mg. The kinetic energy, computed with the initial velocity and the body mass, is 1.23mJ,. In the graph, there is interesting region below 10mg of body mass: in this region, if the mass increases, the jumping height increases because of the effect of the air resistance. This implies an optimum body mass value that achieves the maximum jumping height though the efficiency decreases. In our case, lower mass is better for increasing the jumping performance. In other words, a more powerful actuator will increase jumping height as the gray line (2mJ) in the graph in Fig. 7. The thicker sheet SMA actuator can has the potential to increase the stored elastic energy.

Therefore there are two ways for improving the jumping performance of the jumping robotic insect. The first involves reducing the mass by using lower density materials. However, it is hard to achieve a lower density with same strength as compared to carbon composite plates. The second method is to increase the force of the sheet SMA actuator by using the thicker sheet SMA.

TABLE III. THE AIR DRAG CHARACTERISTICS

Drag Coefficient (C_D)	1.89	
Maximum Jumping Height	In Air (h_a)	30cm
	In Vacuum (h_v) (Simulation)	36cm
Initial Velocity	2.7 m/s	
Jumping Efficiency (h_a/h_v)	0.83	

VI. DISCUSSION

Jumping locomotion using the catapult mechanism is strongly related to the body weight and stored elastic energy. Owing to the effect of air drag, there is an optimal relationship between the body mass and stored energy. In order to meet the optimal design, the actuator and the L-beam design should be modified to increase the stored energy. The body mass can be reduced by using low density materials in the body structures. The novel pop-up book MEMS process may eliminate the onerous assembly task caused by mesoscale components.

This prototype does not have the reflexor actuator for multiple jumping. The reflexor folds the legs back to the initial position for preparing next jump. It can be considered to add the antagonistic actuator or the bias spring as the reflexor muscle on the robot structure.

In the mesoscale robotics, integrated untethered power is a challenging issue. External magnetic fields or bio energy from bacteria can be promising solutions for the locomotion of microrobots in medical applications [15]. However, in our case, the SMA actuator requires thermal energy. Wireless heat transfer such as radiation can be considered to deliver the heat. The activation by an IR laser is one feasible solution for the power of the robot [16].

VII. CONCLUSION

A scalable catapult called the torque reversal mechanism is evolved to be smaller and simpler for a jumping robotic insect. Ongoing research continues to improve the jumping performance and manufacturing process for miniaturization. The current design has a length of 20mm, height of 2mm, weighs 34mg and is capable of jumping about 30cm - roughly

150 times its body height without a tether. Owing to its low mass, the effect of air resistance reduces the jumping efficiency to 0.83, which is similar to that of a real flea (0.8) [5].

This research can be applied to improve traditional mechanical devices such as the end effector of medical robots or a micro mobile robot platform; the jumping mechanism can also be used to produce a rapid snap-though motion in small scale. Microrobotic research including this jumping robotic insect is an effort to expand the capability of robotics by breaking the scale limitation. The development of micro-scale robots has become possible through emerging technologies for downsizing manufacturing and suitable mechanism design.

ACKNOWLEDGMENT

The authors thank K. Ma, Z. E. Teoh, Dr. A. L. Desbiens, M. Smith in Harvard microrobotics Lab. for their constructive discussion and comments and training of various machines.

REFERENCES

[1] M. Noh, S. Kim, S. An, J. Koh and K. Cho, "Flea-Inspired Catapult Mechanism for Miniature Jumping Robots", *Robotics, IEEE Transactions on (TRO)*, vol. 28, no. 5, pp. 1007-1018, Oct. 2012.

[2] J. Koh, S. Jung, M. Noh, S. Kim and K. Cho, "Flea Inspired Catapult Mechanism with Active Energy Storage and Release for Small Scale Jumping Robot", in *Conf. 2013 IEEE Int. Conf. Robotics and Automation (ICRA2013),* To appear.

[3] R. J. Wood, S. Avadhanula, R. Sahai, E. Steltz, and R. S. Fearing, "Microrobot Design Using Fiber Reinforced Composites," *Journal of Mechanical Design*, vol. 130, no. 5, pp. 052304-11, 2008.

[4] P. S. Sreetharan, J. P. Whitney, M. D. Strauss and R. J. Wood, "Monolithic fabrication of millimeter-scale machines", *Journal of Micromechanics and Microengineering*, vol 22, no 5, p 055027, 5 2012.

[5] H. C. Bennet-Clark and G. M. Alder, "The Effect of Air Resistance on the Jumping Performance of Insects", *J Exp Biol*, vol 82, no 1, pp 105–121, 1 1979.

[6] U. Scarfogliero, C. Stefanini, and P. Dario, "The use of compliant joints and elastic energy storage in bio-inspired legged robots," *Mechanism and Machine Theory*, vol. 44, no. 3, pp. 580-590, 2009.

[7] M. Kovač, M. Fuchs, A. Guignard, J.-C. Zufferey, and D. Floreano, "A miniature 7g jumping robot," in *Proc. IEEE International Conference on Robotics and Automation*, 2008, pp. 373-378.

[8] A. Yamada, M. Watari, H. Mochiyama, and H. Fujimoto, "An asymmetric robotic catapult based on the closed elastica for jumping robot," in *Proc. IEEE International Conference on Robotics and Automation*, 2008, pp. 232-237.

[9] R. Armour, K. Paskins, A. Bowyer, J. Vincent, and W. Megill, "Jumping robots: A biomimetic solution to locomotion across rough terrain," *Bioinspiration and Biomimetics*, vol. 2, no. 3, pp. S65-S82, 2007.

[10] B. G. A. Lambrecht, A. D. Horchler, and R. D. Quinn, "A small, insect-inspired robot that runs and jumps," in *Proc. IEEE International Conference on Robotics and Automation*, 2005, pp. 1240-1245.

[11] J. Zhao, N. Xi, B. Gao, M. W. Mutka and L. Xiao, "Development of a controllable and continuous jumping robot", *in 2011 IEEE International Conference on Robotics and Automation (ICRA)*, 2011, pp 4614–4619.

[12] Y. Matsuyama and S. Hirai, "Analysis of circular robot jumping by body deformation," in *Proc. IEEE International Conference on Robotics and Automation*, 2007, pp. 1968-1973.

[13] S. Bergbreiter and K. S. J. Pister, "Design of an autonomous jumping microrobot," in *Proc. IEEE International Conference on Robotics and Automation*, 2007, pp. 447-453.

[14] P. Fiorini and J. Burdick, "The development of hopping capabilities for small robots," *Autonomous Robots*, vol. 14, no. 2-3, pp. 239-254, 2003.

[15] M. Sitti, "Miniature devices: Voyage of the microrobots", *Nature*, vol 458, no 7242, pp 1121–1122, 4 2009.

[16] S. C. Ryu, Z. F. Quek, P. Renaud, R. J. Black, B. L. Daniel and M. R. Cutkosky, "An optical actuation system and curvature sensor for a MR-compatible active needle"*, in 2012 IEEE International Conference on Robotics and Automation (ICRA)*, 2012, pp 1589 –1594.